

# Structure of a Potential Therapeutic Antibody Bound to Interleukin-16 (IL-16)

## MECHANISTIC INSIGHTS AND NEW THERAPEUTIC OPPORTUNITIES\*<sup>‡</sup>

Received for publication, December 16, 2015, and in revised form, April 8, 2016 Published, JBC Papers in Press, May 26, 2016, DOI 10.1074/jbc.M115.709303

Gareth Hall<sup>†1</sup>, Eilish Cullen<sup>§</sup>, Kovilen Sawmynaden<sup>§</sup>, Joanne Arnold<sup>§</sup>, Simon Fox<sup>§</sup>, Richard Cowan<sup>‡</sup>, Frederick W. Muskett<sup>‡</sup>, David Matthews<sup>§2</sup>, Andrew Merritt<sup>§</sup>, Catherine Kettleborough<sup>§</sup>, William Cruikshank<sup>¶</sup>, Debra Taylor<sup>§</sup>, Richard Bayliss<sup>‡</sup>, and Mark D. Carr<sup>†3</sup>

From the <sup>†</sup>Department of Molecular and Cell Biology, Henry Wellcome Building, University of Leicester, Leicester, LE1 9HN, United Kingdom, <sup>§</sup>MRC Technology, Centre for Therapeutics Discovery, 1-3 Burtonhole Lane, Mill Hill, London NW7 1AD, United Kingdom, and the <sup>¶</sup>Boston University School of Medicine, Boston, Massachusetts 02118

Interleukin-16 (IL-16) is reported to be a chemoattractant cytokine and modulator of T-cell activation, and has been proposed as a ligand for the co-receptor CD4. The secreted active form of IL-16 has been detected at sites of T<sub>H</sub>1-mediated inflammation, such as those seen in autoimmune diseases, ischemic reperfusion injury (IRI), and tissue transplant rejection. Neutralization of IL-16 recruitment to its receptor, using an anti-IL16 antibody, has been shown to significantly attenuate inflammation and disease pathology in IRI, as well as in some autoimmune diseases. The 14.1 antibody is a monoclonal anti-IL-16 antibody, which when incubated with CD4<sup>+</sup> cells is reported to cause a reduction in the T<sub>H</sub>1-type inflammatory response. Secreted IL-16 contains a characteristic PDZ domain. PDZ domains are typically characterized by a defined globular structure, along with a peptide-binding site located in a groove between the  $\alpha$ B and  $\beta$ B structural elements and a highly conserved carboxylate-binding loop. In contrast to other reported PDZ domains, the solution structure previously reported for IL-16 reveals a tryptophan residue obscuring the recognition groove. We have solved the structure of the 14.1Fab fragment in complex with IL-16, revealing that binding of the antibody requires a conformational change in the IL-16 PDZ domain. This involves the rotation of the  $\alpha$ B-helix, accompanied movement of the peptide groove obscuring tryptophan residue, and consequent opening up of the binding site for interaction. Our study reveals a surprising mechanism of action for the antibody and identifies new opportunities for the development of IL-16-targeted therapeutics, including small molecules that mimic the interaction of the antibody.

Interleukin-16 (also known as lymphocyte chemoattractant factor) was first described in 1982 as a T-cell chemoattractant

factor produced by antigen and mitogen-stimulated lymphocytes (1). An array of immune and non-immune cells are now known to express IL-16 as one aspect of an inflammatory response, including CD4<sup>+</sup> and CD8<sup>+</sup> T cells, eosinophils, monocytes, mast cells, and dendritic cells (2–5). In addition, IL-16 has been reported to promote the entry of resting CD4<sup>+</sup> T cells into the cell cycle, and the up-regulation of IL-2 receptor and major histocompatibility (MHC) class II proteins on cell surfaces (6, 7).

Human IL-16 (hIL-16)<sup>4</sup> is expressed as a 631-amino acid precursor protein and contains three PDZ domains, along with an N-terminal CcN motif, encompassing both CK2 and cdc2 kinase phosphorylation sites, a nuclear localization signal, and an Src homology 3 binding motif (Fig. 1A) (8, 9). Following cytosolic proteolysis of hIL-16 by caspase-3, a 121-amino acid fragment encompassing the C-terminal PDZ domain (residues 527–619) is secreted as the mature form of IL-16 (10). Secreted IL-16 has been reported to bind to CD4 with relatively high affinity (6, 11, 12), which is consistent with IL-16 functioning as a pro-inflammatory cytokine. The protein is reported to have two major effects on CD4<sup>+</sup> cells: chemoattraction, preferentially of T<sub>H</sub>1 cells, and inhibition of CD3/T-cell mediated activation, preferentially of T<sub>H</sub>2 cells (13). Co-incubation of CD4<sup>+</sup> cells with an anti-CD4 antibody (OKT4) is reported to lead to a reduction in the magnitude of IL-16-induced cell migration by monocytes (11). The protein CD4 contains four immunoglobulin (Ig)-like domains (D1–D4), and CD4-derived peptide inhibition studies of IL-16-mediated chemotaxis suggested that IL-16 binds to CD4 D4 (6). There is also evidence to suggest that chemokine receptor 5, which is expressed on the surface of T<sub>H</sub>1 cells, enhances the binding of IL-16 to the co-receptor (14).

Interestingly, the chemotactic activity of hIL-16 is not associated with a characteristic chemokine structural motif (15, 16). The solution structure of mature hIL-16 has been reported and showed the chemokine to contain a classical PDZ domain, consisting of a central up and down  $\beta$ -sandwich, adjacent to an  $\alpha$ -helix (17). PDZ domains typically assist in the assembly of multiprotein signaling complexes, by binding peptides in a groove between the  $\alpha$ 1-helix and  $\beta$ 2-strand, in a process known

\* The authors declare that they have no conflicts of interest with the contents of this article.

<sup>‡</sup> This article contains supplemental Figs. S1–S3.

The atomic coordinates and structure factors (code 5FB8) have been deposited in the Protein Data Bank (<http://www.pdb.org/>).

<sup>1</sup> To whom correspondence may be addressed. Tel.: 0116-229-7077; E-mail: gh126@le.ac.uk.

<sup>2</sup> To whom correspondence may be addressed. Tel.: 020-8906-7100; E-mail: david.matthews@tech.mrc.ac.uk.

<sup>3</sup> To whom correspondence may be addressed. Tel.: 0116-229-7075; E-mail: mdc12@le.ac.uk.

<sup>4</sup> The abbreviations used are: IL-16, interleukin-16; CD4, cluster of differentiation 4; CDR, complementarity determining region; Bistris propane, 1,3-bis[tris(hydroxymethyl)methylamino]propane.

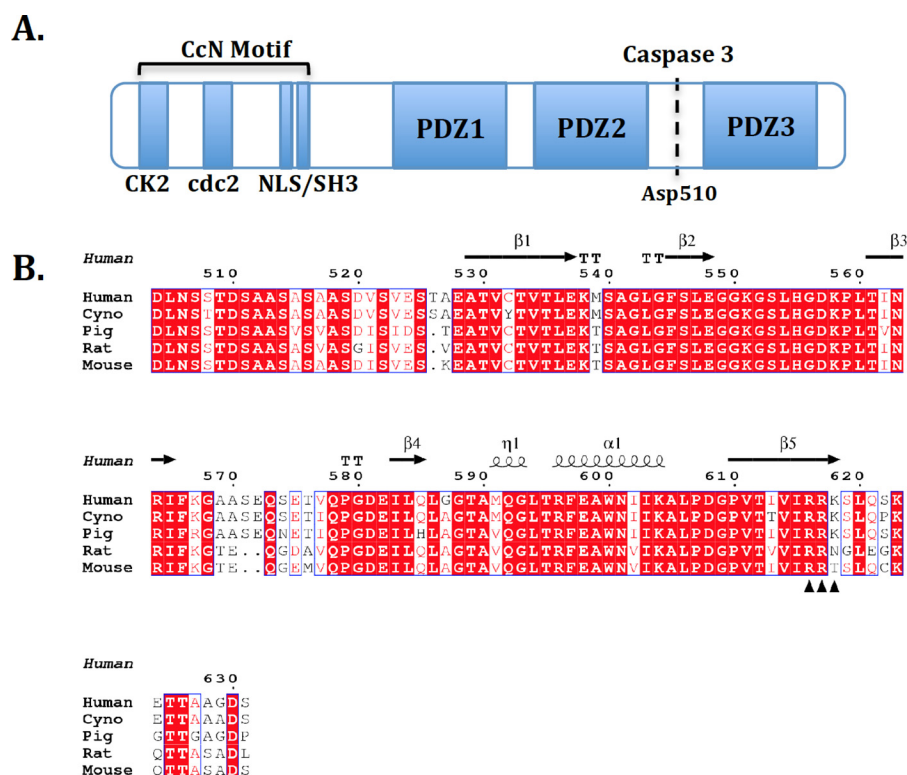


**FIGURE 1. IL-16 domain structure.** A, IL-16 is expressed as a 631-amino acid precursor protein comprising an N-terminal CcN motif and three C-terminal PDZ domains. Caspase-3 cleaves the precursor protein at Asp<sup>510</sup>, between PDZ domains 2 and 3, releasing the mature secreted IL-16 component (2). B, multiple sequence alignment of secreted mammalian IL-16 proteins, revealing high sequence homology in the  $\beta$ 2 to  $\beta$ 3 strand and  $\alpha$ 1-helix regions. The secondary structure based on human IL-16 is shown above. With the exception of the  $\beta$ 3/ $\beta$ 4 loop region, the core of the protein has very high sequence homology across all mammalian species. Putative CD4 binding site residues highlighted (\*). The figure was prepared using ESPript 3.0 (46).

as  $\beta$ -strand addition (18). This peptide recognition is mediated by a conserved GLGF motif termed the “carboxylate-binding loop,” which coordinates a number of hydrogen bonds to the C-terminal carboxylate of the binding peptide. Surprisingly, the typical PDZ-peptide binding groove is blocked by an aromatic side chain in the reported hIL-16 structure, despite conservation of the GLGF motif.

There is high sequence homology for IL-16 across mammalian species, with over 85% sequence similarity between human and murine IL-16. The extent of the conservation is even higher at the C-terminal peptide-binding interface associated with typical PDZ activity (Fig. 1B), strongly suggesting a conserved functional importance. However, the reported tight interaction between IL-16 and CD4 ( $K_d = 230$  pM) has been proposed to involve a cluster of residues close to the C terminus of IL-16 (<sup>616</sup>RRKS<sup>619</sup>) (14, 19) (Fig. 1B).

IL-16 is associated with disease pathogenesis in a number of autoimmune conditions, with expression levels raised in serum from patients with rheumatoid arthritis, multiple sclerosis, and systemic lupus erythematosus (15, 20, 21). The incubation of dendritic cells with a mouse anti-IL-16 monoclonal antibody (mAb 14.1) was reported to result in a significant reduction in cell migration in cultures of epidermal cells (22). Furthermore, neutralization of hIL-16 by mAb 14.1 produced a reduction in the T<sub>H</sub>1-type inflammatory response (2) and the mAb 14.1 antibody has shown *in vivo* efficacy in a rodent model of acute kidney injury (23). The potential of hIL-16 as a therapeutic target in a range of autoimmune conditions has led to the devel-

opment of a panel of inhibitory monoclonal antibodies. In this communication we report the structure of a promising Fab candidate (c14.1) based on mAb 14.1 bound to hIL-16, which reveals an unexpected binding site for the inhibitory antibody on the opposite face of the protein to the proposed CD4 binding site. In addition, the structure of the c14.1Fab·IL-16 complex reveals a significant conformational change in hIL-16, allowing residues from the CDR loops to make extensive contacts in the generic PDZ domain peptide-binding groove. This raises the possibility of the IL-16 PDZ domain modifying its activity via a cryptic peptide binding site. The structural changes induced in hIL-16 by the inhibitory antibody binding also reveal new opportunities for the design of small molecule inhibitors to target hIL-16 activity.

## Experimental Procedures

**Expression and Purification of hIL-16**—A recombinant protein corresponding to mature secreted human IL-16 (residues 502–631) with an N-terminal His<sub>6</sub> tag was expressed as a soluble product using a pLEICS-01 vector (Protex, University of Leicester) transformed into the *Escherichia coli* strain BL21 (DE3) (Novagen). Uniformly <sup>13</sup>C/<sup>15</sup>N/<sup>2</sup>D- and <sup>15</sup>N-labeled hIL-16 were prepared by growing at 37 °C in modified Spizizen minimal medium (24, 25) containing <sup>15</sup>NH<sub>4</sub>SO<sub>4</sub> (4 g liter<sup>-1</sup>) and/or [<sup>13</sup>C<sub>6</sub>]glucose (2 g liter<sup>-1</sup>) as required, with deuterated samples grown in media dissolved in 100% D<sub>2</sub>O. The protein was purified to homogeneity by chromatography on affinity (nickel-nitrilotriacetic acid column, Qiagen) and gel filtration

## Structure of Interleukin-16 Bound to the 14.1 Antibody

(Superdex 75 16/60, GE Healthcare) columns, into a final buffer of 25 mM phosphate, pH 7.0, 100 mM NaCl, 100  $\mu$ M EDTA, 1 mM DTT, 2 mM MgCl<sub>2</sub>, and 1 mM imidazole. The His tag was removed prior to gel filtration using tobacco etch virus protease overnight at 4 °C.

**Expression and Purification of Truncated hIL-16 (hIL-16tr)**—The DNA construct for the truncated form of human IL-16 (IL-16tr, residues 523–622) with an N-terminal His tag was cloned into pLEICS-01 and transformed in *E. coli* BL21 cells. The soluble protein was expressed in 2 $\times$  YT media at 18 °C and purified to homogeneity by chromatography on affinity (nickel-nitrilotriacetic acid column, Qiagen) and gel filtration (Superdex 75 16/60, GE Healthcare) columns, into a final buffer of 20 mM Tris-HCl, pH 7.4, 50 mM NaCl, and 1 mM DTT. The His tag was removed prior to gel filtration using tobacco etch virus protease overnight at 4 °C.

**Expression and Purification of the Anti-IL-16 c14.1Fab**—The variable domains from the heavy and light chains of the parent murine anti-IL-16 antibody (14.1) were identified by sequence analysis and subcloned into in-house pCMV-based vectors, containing a C-terminal reading frame for either the first constant domain of human IgG1 (C<sub>H1</sub>) or the human  $\kappa$  constant domain (C<sub>L</sub>), respectively. For expression of the c14.1Fab, the two plasmids encoding the heavy and light chain fragments were transiently co-transfected into Expi293F<sup>TM</sup> cells (Invitrogen) according to the manufacturer's instructions. Cell cultures were maintained for 7–10 days in Expi293<sup>TM</sup> medium at 37 °C (130 rpm and  $\leq$ 8% CO<sub>2</sub> in humidified air) before supernatants were harvested by centrifugation, filter-sterilized (Stericup<sup>®</sup>; Merck Millipore), and stored at 4 °C until required. The secreted c14.1Fab was purified by affinity chromatography, with the harvested supernatant loaded onto a 1-ml KappaSelect column (GE Healthcare) pre-equilibrated with phosphate-buffered saline, pH 7.4, (PBS) and the bound antibody was eluted by 0.1 M glycine, pH 2.5–3.0. The final sample was desalted and buffer exchanged into PBS using a PD10 column (GE Healthcare).

**Expression and Purification of Extracellular Regions of Human CD4 (hCD4)**—DNA inserts comprising hCD4 domains D1–D4 (residues 1–388) and hCD4 D3D4 (residues 202–388) were synthesized and cloned into pcDNA3 (Life Technologies). The hCD4 D3D4 insert also incorporated an additional N-terminal Ig $\kappa$  leader sequence to facilitate protein secretion. Both expression vectors also included a C-terminal His<sub>6</sub> tag to enable affinity-based protein purification. For recombinant hCD4 expression, Expi293F<sup>TM</sup> cells (Life Technologies) were transiently transfected with plasmid DNA according to the manufacturer's instructions and cell cultures (0.2 liter) were maintained for 7–8 days in Expi293<sup>TM</sup> medium at 37 °C (130 rpm and  $\leq$ 8% CO<sub>2</sub> in humidified air). Supernatants were harvested by centrifugation, filter-sterilized (Stericup<sup>®</sup>; Merck Millipore), and subsequently stored at 4 °C. The two hCD4 extracellular region proteins (D1–D4 and D3D4) were purified to homogeneity using a HisTrap-excel column (GE Healthcare) and by size exclusion chromatography using either a Superdex 75 (16/60; GE Healthcare) or Superdex 200 (26/60; GE Healthcare), as appropriate, into a final buffer of PBS.

**Complex Preparation**—The c14.1Fab-IL-16 and c14.1Fab-IL-16tr complexes were prepared by mixing the c14.1Fab with either hIL-16 or hIL-16tr at a Fab:IL-16 molar ratio of 1.2:1. The mixtures were incubated for 60 min at 4 °C, concentrated with a Vivaspın-20 to a final volume of 2.0 ml, and purified on a Superdex 75 16/60 column (GE Healthcare). The running buffer used was either 25 mM phosphate, pH 7.0, 100 mM NaCl, 100  $\mu$ M EDTA, 1 mM DTT, and 1 mM imidazole or 20 mM Tris-HCl, pH 7.4, and 50 mM NaCl, for the c14.1Fab-IL-16 and c14.1Fab-IL-16tr complexes, respectively. Fractions corresponding to the protein complex peak in each case were pooled and concentrated for NMR and crystallographic studies with a Vivaspın-20. As expected, the complex formation in both cases resulted in a significant shift in retention time on a Superdex 75 column compared with that for the free c14.1Fab and hIL-16.

**NMR Spectroscopy**—All NMR data were acquired on Bruker Avance III 600 and 800 MHz spectrometers equipped with 5-mm HCN cryoprobes. Both the hIL-16 and c14.1Fab-hIL-16 NMR samples were prepared at 150  $\mu$ M in 25 mM sodium phosphate buffer, pH 7.0, containing 100 mM NaCl, 100  $\mu$ M EDTA, 1 mM DTT, and 1 mM imidazole in 90% H<sub>2</sub>O, 10% D<sub>2</sub>O. The two-dimensional <sup>15</sup>N-<sup>1</sup>H TROSY spectra of hIL-16 were obtained at 25 and 35 °C, in the absence or presence of c14.1Fab, respectively. Typical acquisition times for the triple resonance experiments were 80 ms in F<sub>3</sub> (<sup>1</sup>H), 22 ms in F<sub>2</sub> (<sup>15</sup>N), and 6 or 25 ms in F<sub>1</sub> (<sup>13</sup>C) as appropriate, with the spectra collected over ~13–60 h. All datasets were non-uniform sampled to 25% and reconstructed using hms1ST software (26). Backbone amide chemical shifts for free hIL-16 were consistent with those reported previously. However, all backbone assignments were confirmed using three-dimensional HNCO, CBCACONH, and CBCANH experiments, allowing for the full assignment of peaks from the <sup>15</sup>N-<sup>1</sup>H TROSY spectra. All NMR data were processed and analyzed using NMRPipe (27) and SPARKY (University of California, San Francisco, CA) software.

The minimal shift approach (28) was used to identify hIL-16 residues involved in c14.1Fab binding. Backbone amide minimal shift values were obtained from the combined chemical shift change in <sup>15</sup>N and <sup>1</sup>H for each assigned peak in the <sup>15</sup>N/<sup>1</sup>H TROSY spectrum of the free <sup>15</sup>N-labeled hIL-16, when compared with all peaks observed in the <sup>15</sup>N/<sup>1</sup>H TROSY spectrum of the <sup>15</sup>N-labeled hIL-16 bound to unlabeled c14.1Fab. A histogram of combined minimal shift *versus* protein sequence revealed residues from hIL-16 with backbone amide signals significantly perturbed by antibody binding.

**Protein Crystallography**—Initial crystallization trials for the c14.1Fab-IL-16tr complex were performed at 20 mg/ml using sitting drop vapor diffusion and 96-well block screens (Molecular Dimensions) at 20 °C. Optimal crystals of c14.1Fab-hIL-16tr grew in 16% PEG3350, 0.1 M Bistris propane, pH 6.5, and 0.2 M sodium sulfate. A cryoprotectant consisting of 22% (v/v) ethylene glycol in mother liquor was used. X-ray diffraction data were collected at the Diamond Light Source (Oxford, UK) using beamline I03.

Diffraction data were indexed and integrated in Xds (29) and scaled using SCALA (30). A Matthews coefficient (31) calculated one molecule of c14.1Fab and one molecule of hIL-16tr

**TABLE 1**  
X-ray data and refinement statistics

c14.1Fab-hIL-16	
<b>Data collection</b>	
Wavelength (Å)	0.97626
Space group	P2 <sub>1</sub> ,2 <sub>1</sub> ,2 <sub>1</sub>
Cell dimensions	
<i>a</i> , <i>b</i> , <i>c</i> (Å)	59.69, 65.95, 196.44
$\alpha$ , $\beta$ , $\gamma$ (°)	90, 90, 90
Resolution (Å)	29.45–2.07
<i>R</i> <sub>merge</sub>	0.055 (0.695)
<i>I</i> / $\sigma$ <i>I</i>	17.79 (3.44)
Completeness (%)	99.81 (99.85)
Redundancy	6.3 (6.5)
Matthews coefficient	0.983
Solvent content (%)	63.86
<b>Refinement</b>	
No. of reflections	304,909 (22954)
No. of unique reflections	48,100 (4710)
<i>R</i> <sub>factor</sub> / <i>R</i> <sub>free</sub> (%)	17.18 (20.53)
Wilson <i>B</i> -factors (Å <sup>2</sup> )	39.24
<i>B</i> -factors (Å <sup>2</sup> )	
Protein	44.90
Solvent	53.50
Root mean square deviations	
Bond lengths (Å)	0.008
Bond angles (°)	1.15
Ramachandran plot	
Most favored (%)	96.3
Allowed (%)	3.5

present in the asymmetric unit. A homology model of c14.1Fab was generated using SWISSMODEL (32) with the deposited antibody structures Protein Data Bank codes 4F33 (33) and 1I7Z (34), used to model the heavy and light chains, respectively. The structure of the c14.1Fab-hIL-16tr complex was determined by molecular replacement, using the program PHASER (35), with the hIL-16 NMR structure (PDB code 1I16) and the c14.1Fab homology model used in the search. Model building and structural refinement was carried out with Coot (36), PHENIX (37), and REFMAC 5.0 (38) using restrained refinement and isotropic *B*-factors. X-ray data collection and refinement statistics are given in Table 1.

**ELISA-type c14.1mAb-IL-16 Binding Assays**—Wells on streptavidin HBC plates (Thermo Scientific) were coated overnight at 4 °C with 50  $\mu$ l of 0.048–25  $\mu$ g/ml of recombinant hIL-16 or hIL-16 W600A in Dulbecco's PBS (Thermo Scientific). After blocking with 2% BSA in PBS at room temperature for 1 h, 50  $\mu$ l of 1  $\mu$ g/ml of c14.1 antibody in Dulbecco's PBS with 0.1% BSA was added to the wells and incubated for 1 h at room temperature. Following incubation with HRP-conjugated anti-mouse (Fc specific) antibodies (Sigma A2304) (1:5,000 dilution) at room temperature for 1 h, the substrate 3,3',5,5'-tetramethylbenzidine (Sigma, T4444) was added and allowed to develop. Bound proteins were quantified after measuring the absorbance at 450–650 nm in a microtiter plate reader (Tecan Saffire), and data were analyzed by GraphPad Prism software.

**Flow Cytometry Analysis of OKT4 Antibody and hIL-16 Binding to Cell Surface CD4**—Flow cytometry analysis of both hIL-16 and OKT4 antibody binding to cell surface CD4 was performed in duplicate, with  $1 \times 10^5$  cells per well in FACS buffer (PBS + 2% FBS). The OKT4 antibody binds to the D3 domain of CD4. CD4+ve cells were incubated with hIL-16 (3.3 ng/ml to 33 mg/ml) for 2 h at 4 °C, followed by biotinylated OKT4 (eBioscience 13-0048) at 500 ng/ml final concentration and streptavidin Alexa Fluor 488 (Invitrogen, S11223) at 2

$\mu$ g/ml final concentration for 30 min at 4 °C, then analyzed using a Millipore guava easyCyte.

## Results and Discussion

**Mapping the Binding Site of the c14.1Fab on hIL-16**—Residues from hIL-16 significantly perturbed by the interaction with the c14.1Fab were identified by comparison of <sup>15</sup>N/<sup>1</sup>H TROSY spectra acquired for the free and antibody bound protein (Fig. 2). Comprehensive backbone and side chain assignments have been previously reported for hIL-16 (17), and it proved relatively straightforward to obtain nearly complete backbone resonance assignments for free hIL-16 under our experimental conditions. The observed minimal shifts in backbone amide signals of hIL-16 on complex formation are summarized in the histogram shown in Fig. 2A and mapped onto the structure of free hIL-16 to clearly identify a contiguous antibody interaction surface. c14.1Fab binding to hIL-16 results in very significant shifts (N-H  $\Delta\delta \geq 0.15$  ppm) for 15 residues (Gly<sup>542</sup>, Gly<sup>544</sup>, Ser<sup>546</sup>, Gly<sup>549</sup>, Gly<sup>550</sup>, Ser<sup>553</sup>, Asp<sup>557</sup>, Thr<sup>561</sup>, Arg<sup>564</sup>, Met<sup>591</sup>, Arg<sup>596</sup>, Trp<sup>600</sup>, Asn<sup>601</sup>, Ile<sup>603</sup>, and Ala<sup>605</sup>), which form the interaction surface highlighted in Fig. 2B. These residues are predominantly localized to the  $\beta$ 2 and  $\beta$ 3 strands, the  $\beta$ 2/ $\beta$ 3 loop, and the neighboring  $\alpha$ 1-helix, collectively forming a continuous patch of  $\sim 683$  Å<sup>2</sup> on the surface of hIL-16, which is consistent with the size expected for an antibody binding site (39, 40). Surprisingly, the antibody interaction surface identified does not include the residues previously reported to be involved in binding to CD4 (Arg<sup>616</sup>, Arg<sup>617</sup>, and Lys<sup>618</sup>), suggesting that the inhibitory activity of c14.1Fab is not due to direct blocking of CD4 binding to hIL-16.

**Structure of the c14.1Fab-hIL-16 Complex**—To further characterize the interaction of the c14.1Fab with hIL-16 and the molecular basis of the inhibition of activity, the structure of the c14.1Fab-hIL-16 complex was solved by x-ray crystallography to 2.1 Å. The published solution structure of mature hIL-16 (PDB 1I16) revealed highly flexible regions on either end of the central PDZ3 domain (17). In addition, the NMR interaction studies reported here show that these regions are not involved in c14.1Fab binding and that the PDZ3 domain alone contained the entire antibody interaction site. Consequently, an isolated PDZ3 domain hIL-16 construct was prepared corresponding to residues 523–622 (hIL-16tr) and assessed for crystallographic studies. Size exclusion chromatography confirmed that this truncated form of hIL-16 (hIL-16tr) still bound with high affinity to the c14.1Fab molecule and crystals of the antibody-hIL-16tr complex were obtained that diffracted to 2.1 Å.

Analysis of the diffraction data indicated that the crystals contained one molecule of IL-16tr:c14.1Fab complex in the asymmetric unit. Interpretable electron density was obtained for hIL-16tr residues Glu<sup>527</sup> to Ser<sup>619</sup>, c14.1Fab heavy chain (V<sub>H</sub>) residues Glu<sup>1</sup> to Ser<sup>223</sup>, and c14.1Fab light chain (V<sub>L</sub>) residues Asp<sup>1</sup> to Cys<sup>218</sup>. The c14.1Fab is a chimeric version of the mouse derived 14.1 inhibitory anti-IL-16 monoclonal antibody. The sequences of the three complementarily determining regions (CDR) in the light (L1, L2, L3) and heavy chains (H1, H2, and H3) can be classified as L1 (Arg<sup>24</sup>-His<sup>38</sup>), L2 (Tyr<sup>53</sup>-Ser<sup>60</sup>), L3 (Gln<sup>93</sup>-Thr<sup>101</sup>), H1 (Gly<sup>26</sup>-Asn<sup>35</sup>), H2 (Leu<sup>50</sup>-Asp<sup>66</sup>), and H3 (Ser<sup>99</sup>-Tyr<sup>110</sup>), respectively (Chothia numbering sys-

## Structure of Interleukin-16 Bound to the 14.1 Antibody

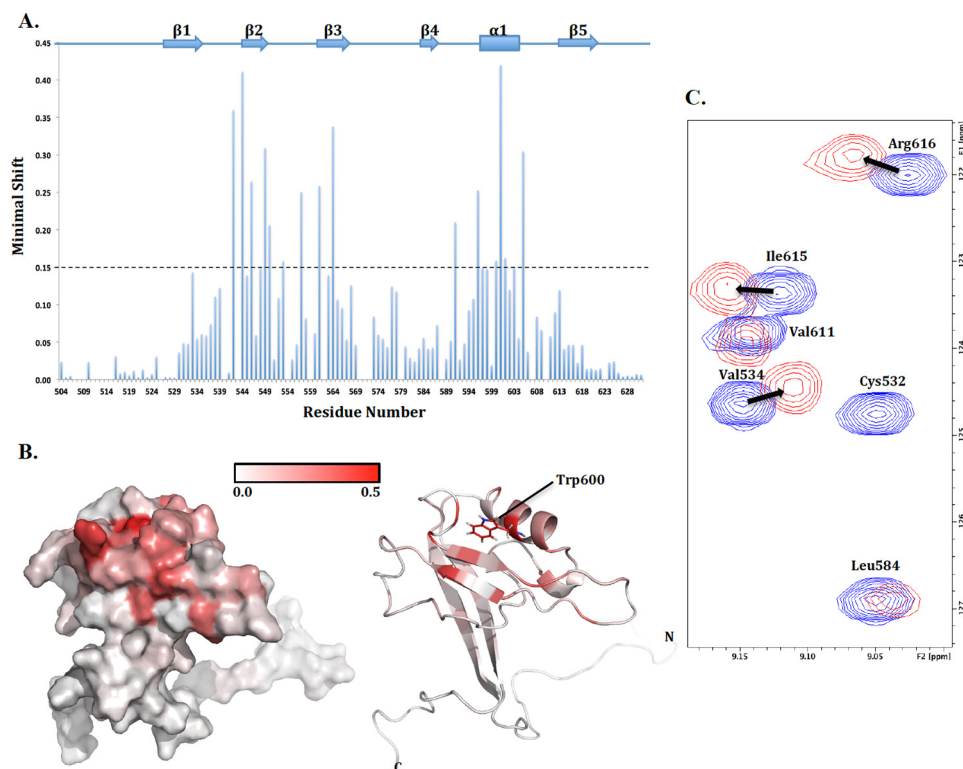


**FIGURE 2. Mapping of the c14.1Fab binding site on hIL-16 by minimal shift NMR analysis.** *A*, histogram revealing the backbone amide minimal shifts seen for the hIL-16 upon complex formation with c14.1Fab. The regions of regular secondary structure are indicated above the plot by blue bars for  $\alpha$ -helices and blue arrows for  $\beta$ -sheets. *B*, mapping of the minimal shift NMR data onto surface and ribbon representations of hIL-16, with significantly perturbed residues (shift  $>0.10$  ppm) colored with a gradient from white to red. Residues for which no minimal shift data were obtained are also shown in white. Residue Trp<sup>600</sup>, experiencing the greatest shift, is highlighted. *C*, a small region from the <sup>15</sup>N-<sup>1</sup>H TROSY spectra of <sup>15</sup>N-labeled hIL-16 both free (blue) and in complex (red) with c14.1Fab, with the assignments for hIL-16 indicated. It is clear that the backbone amide peaks for Val<sup>534</sup>, Ile<sup>615</sup>, and Arg<sup>616</sup> show reasonable shifts, whereas Cys<sup>532</sup> has substantially changed. Images were prepared using PyMol (The PyMOL Molecular Graphics System, version 1.7.4 Schrödinger, LLC.) and Topspin (Bruker Biospin Ltd.).

tem (41)). The structure of the protein complex shows hIL-16tr bound to the conventional antigen binding surface on the c14.1Fab (Fig. 3). The overall structure of the antibody-bound hIL-16tr molecule is very similar to the published hIL-16 free structure ( $C\alpha$  root mean square deviation = 2.09 Å), with the exception of residues 569–575, which appear to be disordered in the crystal structure. The most notable difference in the backbone was for Leu<sup>554</sup> (~10.2 Å in  $C\alpha$  positions), which is situated in the  $\beta 2/\beta 3$  loop that was shown to be dynamic in solution (17). In complex with the c14.1Fab the hIL-16  $\beta 2/\beta 3$  loop interacts with CDR-H1, which is likely to stabilize this loop region of hIL-16 and may induce a change in conformation compared with the free protein.

**Features of the Antibody-IL-16 Interface**—The c14.1Fab-IL-16tr interface buries 876 Å<sup>2</sup> of antibody protein surface from bulk solvent, with 603 Å<sup>2</sup> of the buried surface from the V<sub>H</sub> domain and 273 Å<sup>2</sup> from the V<sub>K</sub> domain. In the case of IL-16 a comparable surface of 853 Å<sup>2</sup> is buried by complex formation. This is consistent with the contact surface area estimated from the NMR studies discussed earlier and lies within the typical range of 850 ± 130 Å<sup>2</sup> for an antibody-binding site on target proteins (39, 40). With the exception of CDR-L3, at least one residue from all CDR loops is within 5 Å of hIL-16, with 22 amino acids from the CDR loops losing at least 10 Å<sup>2</sup> of solvent accessibility and making direct contacts with hIL-16. The extensive interface features a mixture of polar and hydrophobic

contacts, including the involvement of eight aromatic side chains in the CDR loops, from both the V<sub>H</sub> (Tyr<sup>52</sup>, Tyr<sup>74</sup>, Tyr<sup>121</sup>, Tyr<sup>122</sup>, and Tyr<sup>127</sup>) and V<sub>K</sub> (Tyr<sup>59</sup>, Tyr<sup>61</sup>, and Tyr<sup>78</sup>) domains. Of these, all are forming hydrogen bonds through their side chain hydroxyl groups, with the exception of Tyr<sup>59</sup>, Tyr<sup>61</sup>, and Tyr<sup>121</sup>. Examples of the interactions seen between the antibody and hIL-16 are illustrated in Fig. 4.

There are 25 residues from hIL-16 within 5 Å of c14.1Fab in the complex, which form a continuous contact surface comprising  $\beta$ -strands  $\beta 2$  and  $\beta 3$ , the  $\beta 2/\beta 3$  loop, and  $\alpha 1$  helix (Fig. 3B). This antibody binding site on hIL-16 contains many of the residues, which show substantial changes in the backbone amide chemical shifts on complex formation (Fig. 2A and 2B), including residues Gly<sup>542</sup>, Gly<sup>544</sup>, Ser<sup>546</sup>, Ser<sup>553</sup>, Arg<sup>564</sup>, Arg<sup>596</sup>, Trp<sup>600</sup>, and Ile<sup>603</sup>. However, significant shifts in backbone amide signals were also seen for several residues not directly involved in antibody binding such as residues Gly<sup>549</sup>, Gly<sup>550</sup>, Met<sup>591</sup>, Asn<sup>601</sup>, and Ala<sup>605</sup>. This probably reflects the conformational change in hIL-16 induced by antibody binding and discussed below (Fig. 5).

The c14.1Fab interaction surface on hIL-16 includes several basic residues, such as Arg<sup>564</sup> and Arg<sup>596</sup>, which gives the binding site on hIL-16 an overall positive charge. The complementary face of the antibody includes four acidic residues from the CDR loops (Asp<sup>100</sup>, Asp<sup>103</sup>, and Asp<sup>109</sup> from CDR-H3; and Glu<sup>59</sup> from CDR-L2). Of these, Asp<sup>100</sup> and Glu<sup>59</sup> form salt

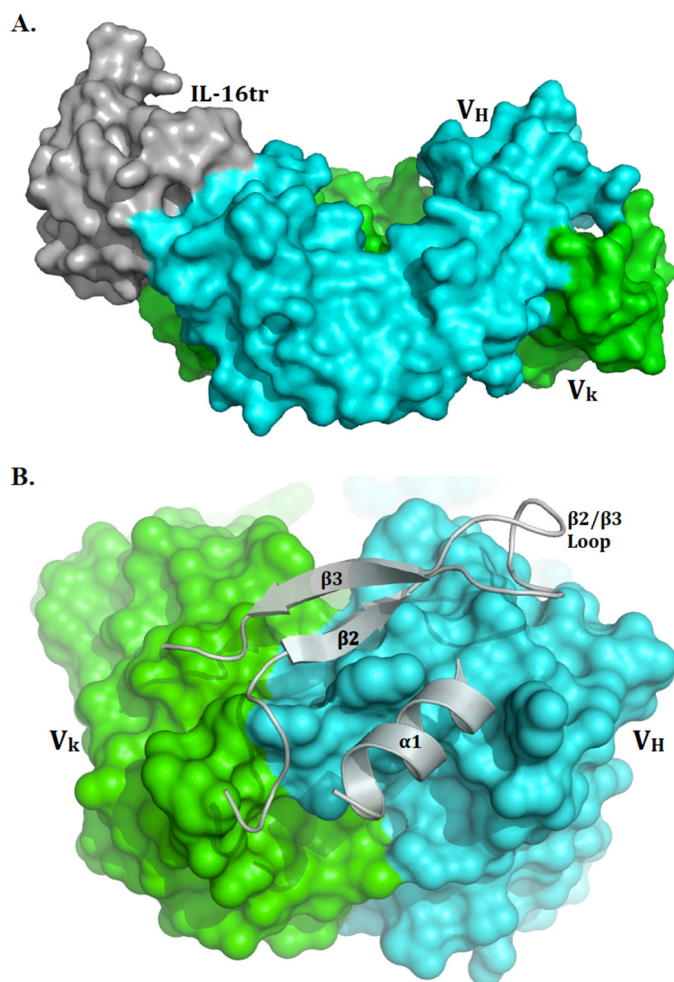


**FIGURE 3. Structure of the c14.1Fab-hIL-16 complex.** *A*, surface representation of hIL-16 (gray) bound to the c14.1Fab, showing the heavy (cyan) and  $\kappa$  (green) chains. *B*, ribbon representation of hIL-16 residues within 5 Å of c14.1Fab heavy (cyan) and  $\kappa$  (green) chains. There are 25 residues from hIL-16 that form a continuous contact surface and comprise of  $\beta$ -strands  $\beta 2$  and  $\beta 3$ , the  $\beta 2/\beta 3$  loop, and  $\alpha 1$  helix.

bridges with Arg<sup>596</sup> and Arg<sup>564</sup>, respectively, as illustrated for Asp<sup>100</sup> and Arg<sup>596</sup> in Fig. 4*B*, and which contributes to both the specificity and stability of the complex formed. In total there are 10 salt bridges and hydrogen bonds between hIL-16 and c14.1Fab, together with 13 bridging water molecules, which collectively form a complex hydrogen-bonding and ionic interaction lattice between the two proteins.

A major contributor to the specificity and affinity of the recognition of hIL-16 by the c14.1Fab is shape complementarity at the center of the binding site, driven predominantly by residues in CDR-H3 (Tyr<sup>101</sup>, Tyr<sup>102</sup>, and Asp<sup>103</sup> (Fig. 4)). These CDR residues occupy the GLGF cleft on hIL-16, which is a structural feature typical of PDZ domains that commonly bind C-terminal peptides (42). The previously reported solution structure of free hIL-16 indicated that this cleft on the hIL-16 was too small to accommodate peptide binding or other potential ligands and was also occluded by the indole side chain of Trp<sup>600</sup>. In addition, there was no evidence of significant mobility of this region in the free hIL-16 solution structures, nor have any peptides been identified that bind to IL-16. Interestingly, the structure of the c14.1Fab-hIL-16 complex reveals a significant antibody-in-

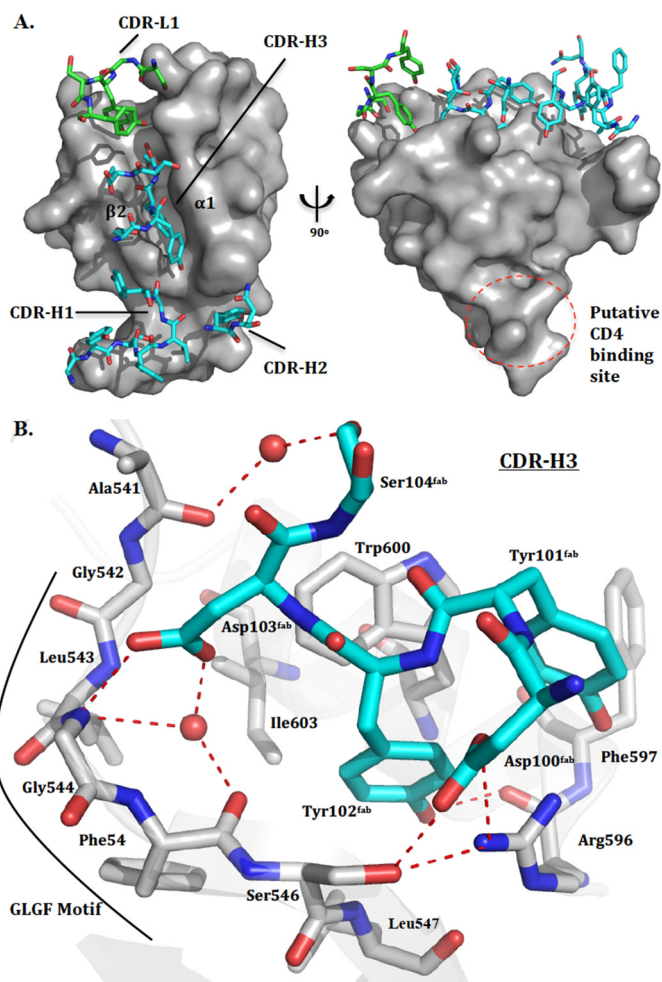


**FIGURE 4. Summary of the molecular interactions between hIL-16 and c14.1Fab.** *A*, surface representation of hIL-16 (gray) and stick representation of CDR loops from c14.1Fab from the heavy (cyan) and  $\kappa$  (green) chains. The interacting CDR loops follow the PDZ groove between the  $\alpha 1$ -helix and  $\beta 2$ -strand. The c14.1Fab epitope revealed is distant to the putative CD4 binding site. *B*, stick representation of CDR-H3 from c14.1Fab interacting with the putative functional paratope of hIL-16, including the PDZ pocket and the GLGF cleft region. Tyr<sup>102</sup> from CDR-H3 fits into the IL-16 PDZ pocket, formed by residues Phe<sup>545</sup>, Ser<sup>546</sup>, Leu<sup>547</sup>, Arg<sup>596</sup>, Ala<sup>599</sup>, Trp<sup>600</sup>, and Ile<sup>603</sup>. The acidic side chain of Asp<sup>103</sup> from CDR-H3 forms a hydrogen bond with the amide backbone of Gly<sup>544</sup>, in a similar manner to the carboxyl terminus of a typical peptide binding to the GLGF recognition motif of a PDZ domain.

duced conformational change in the GLGF region of hIL-16, which allows this cleft to accommodate residues from CDR-H3. The localized structural changes observed include a 2 Å shift of the  $\beta 2$ -strand to widen the binding site, and a 30° rotation of the  $\alpha 1$ -helix to lever the Trp<sup>600</sup> side chain from the blocked recognition groove (Fig. 5). These antibody-induced conformational changes in bound hIL-16 permit the phenolic side chain of Tyr<sup>102</sup> from CDR-H3 to occupy the remodeled hIL-16 GLGF cleft, formed by Phe<sup>545</sup>, Ser<sup>546</sup>, Leu<sup>547</sup>, Arg<sup>596</sup>, Ala<sup>599</sup>, Trp<sup>600</sup>, and Ile<sup>603</sup> (Fig. 4*B*). Furthermore, the acidic side chain of Asp<sup>103</sup> from CDR-H3 is now able to form a hydrogen bond with the amide backbone of Gly<sup>544</sup> in a similar interaction to that seen for peptides binding to the GLGF recognition motif of typical PDZ domains (42). Although the interactions seen between c14.1Fab and hIL-16 do not exactly mimic a typical peptide-PDZ domain complex, the similarities suggest that IL-16 may have the function to bind specific peptides or perhaps more

## Structure of Interleukin-16 Bound to the 14.1 Antibody

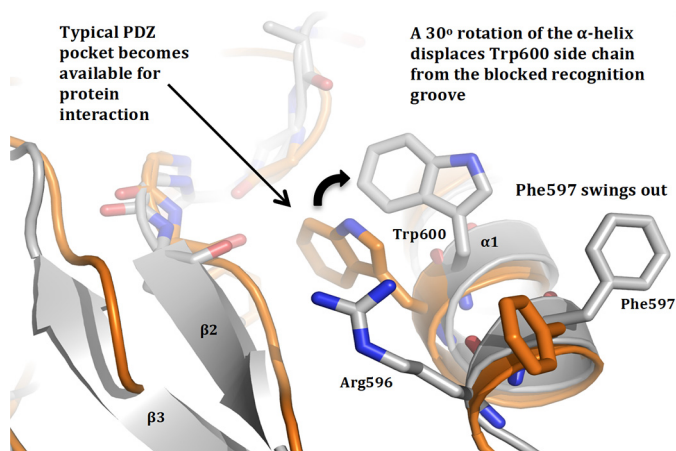


**FIGURE 5. Induced conformational changes to hIL-16 following c14.1Fab binding.** Stick and schematic representation of hIL-16 before (orange) and after (gray) c14.1Fab binding. The interaction between hIL-16 and c14.1Fab results in a 30 degree rotation of the  $\alpha$ 1-helix, displacing Trp<sup>600</sup> from the blocked PDZ recognition groove and opening a pocket for Tyr<sup>102</sup> from CDR-H3 to bind. The  $\alpha$ 1-helix rotation also leads to a conformational change to Phe<sup>597</sup>, forming a hydrophobic groove for Tyr<sup>101</sup> from CDR-H3 to pack against. These conformational shifts in hIL-16 result in the formation of a typical PDZ pocket to permit protein-protein interactions, suggesting that this conformational change may be associated with the biological activity of hIL-16.

likely is that a more substantial interface formed with a protein partner could include a peptide moiety binding within this site as part of a larger contact surface area. Indeed, a conformational change of a PDZ domain to accommodate an interaction partner has been observed previously in the Crb<sup>17</sup> peptide binding to the Pals1 PDZ domain (43). In this instance, Phe<sup>318</sup> (occupying the same position as Trp<sup>600</sup> in hIL-16) sterically blocks the PDZ-binding groove in the ligand-free structure, but adopts a different rotomer conformation away from the groove to accommodate the Crb<sup>17</sup> peptide. Furthermore, the phenyl side chain of Phe<sup>318</sup> packs against residues Arg<sup>1404</sup> and Leu<sup>1405</sup> from Crb<sup>17</sup>, forming one side of the pocket into which the peptide binds.

**Potential Importance of Trp<sup>600</sup> in Target Recognition**—To further probe the importance of the Trp<sup>600</sup> side chain in regulating the binding of target protein/peptides to the GLGF region of hIL-16 we produced a W600A variant of hIL-16 and determined the effects on c14.1 antibody binding using an ELISA-based assay. The hIL-16 W600A mutation resulted in a substantial change in the affinity of the interaction between the c14.1 antibody and hIL-16. Removing the blocking tryptophan side chain by substituting the residue with alanine might be expected to increase the affinity of the c14.1 antibody to hIL-16. However, the affinity was observed to decrease by  $\sim$ 10-fold, from an EC<sub>50</sub> of 115 nM for native hIL-16 (supplemental Fig. S1). This suggests that the energetic penalty arising from the conformational change induced in hIL-16 on antibody binding is more than offset by the network of Van de Waals interactions between the c14.1Fab CDR-H3 loop residues and the hydrophobic pocket formed by hIL-16 residues Phe<sup>545</sup>, Leu<sup>547</sup>, Arg<sup>596</sup>, Ile<sup>603</sup>, and, most importantly, the indole side chain from Trp<sup>600</sup> (Fig. 4B).

**Impact of the c14.1Fab on IL-16 Signaling**—The location of the CD4 binding site on hIL-16 was previously probed by

assessing the inhibition of IL-16-mediated chemotaxis by linear peptides derived from IL-16, which suggested a role for the <sup>616</sup>RRKS<sup>619</sup> motif (19). This putative CD4 binding site is located on the opposite face of hIL-16 to the c14.1Fab binding site reported here. This raises intriguing questions regarding the mechanistic basis of the inhibitory activity of the 14.1 antibody.

Minimal shift NMR experiments were used to assess the binding of CD4 domains D1–D4 and CD4 D3D4 to <sup>15</sup>N-labeled hIL-16 and to establish if CD4 binding was affected by c14.1Fab binding. Surprisingly, in samples with a 5:1 molar excess of either CD4 D1–D4 or D3D4 we observed no shifts in the backbone amide signals of hIL-16, indicating no significant interaction between the two proteins under the experimental conditions used (supplemental Fig. S2). In agreement with the previously published NMR structural studies of hIL-16, the line widths of the backbone amide NMR signals observed are consistent with a predominantly monomeric hIL-16. Interestingly, some reports suggest that CD4 only binds to multimeric forms of hIL-16 (44), however, the inhibitory c14.1Fab clearly binds to monomeric hIL-16 with high affinity.

Attempts to directly or indirectly observe hIL-16 binding to cell lines expressing CD4 by flow cytometry also detected no interaction between CD4 and hIL-16 (supplemental Fig. S3). Fluorescence-activated cell sorting (FACS) experiments showed that recombinant hIL-16 was unable to compete off bound anti-CD4 antibody OKT4, despite concentrations of hIL-16 up to 100 mg/ml. Previous studies have suggested that IL-16 dimerization or tetramerization may be a requirement for CD4 binding and chemoattractant activity, which could account for the lack of CD4 binding observed here, however, it is unclear as to why mammalian expressed IL-16 would be multimeric. The purified mature hIL-16 expressed in *E. coli* and used for the work reported here shows no tendency to form multimeric species at concentrations over 1 mM, which may suggest that the multimeric forms of hIL-16 reported in mammalian cell extracts may involve other protein partners. However, the inhibitory c14.1Fab clearly binds with high affinity to the *E. coli* expressed hIL-16 monomer and neither sterically blocks or perturbs the proposed CD4-binding site on hIL-16.

**Structure-based Design of Small Molecules to Target the IL-16 Functional Site Recognized by c14.1Fab**—The innovative use of antibodies and antibody fragments to identify opportunities for small molecule drug development on a range of proteins selected as attractive therapeutic targets has been proposed recently (45). This includes the identification of antibodies that modulate target protein activity by binding to regulatory sites, with structures obtained for these antibody-target protein complexes used to inform and guide the development of small molecule inhibitors or activators as potential drugs. The structural studies of the c14.1Fab-hIL-16 complex reported here represent an excellent example of the potential of antibody-assisted approaches, with the conformational changes induced by antibody binding revealing new opportunities for small molecule modulation of IL-16 activity. This method of probing the surface of target proteins, using antibodies as tools, to find allosteric and functional pockets is an innovative and exciting prospect and has the potential to revolutionize drug discovery for a wide range of protein targets.

**Author Contributions**—G. H., A. M., C. K., R. B., and M. C. coordinated the study. G. H. and M. C. wrote the paper. G. H. and R. C. purified IL-16 protein, E. C., J. A., and K. S. purified c14.1Fab and CD4 proteins, and G. H. determined the c14.1Fab:IL-16tr complex X-ray structure. G. H. and F. M. designed, performed and analyzed the NMR experiments shown in Fig. 2 and [supplemental Fig. S2](#). J. A. designed and performed the ELISA shown in [supplemental Fig. S1](#). W. C. provided the c14.1Fab DNA construct. S. F. and D. T. designed, performed, and analyzed the FACS experiments shown in [supplemental Fig. S3](#). All authors reviewed the results and approved the final version of the manuscript.

## References

- Cruikshank, W., and Center, D. M. (1982) Modulation of lymphocyte migration by human lymphokines: II. purification of a lymphotactic factor (LCF). *J. Immunol.* **128**, 2569–2574
- Cruikshank, W., and Little, F. (2008) Interleukin-16: the ins and outs of regulating T-cell activation. *Crit. Rev. Immunol.* **28**, 467–483
- Lim, K. G., Wan, H. C., Bozza, P. T., Resnick, M. B., Wong, D. T., Cruikshank, W. W., Kornfeld, H., Center, D. M., and Weller, P. F. (1996) Human eosinophils elaborate the lymphocyte chemoattractants: IL-16 (lymphocyte chemoattractant factor) and RANTES. *J. Immunol.* **156**, 2566–2570
- Rumsaeng, V., Cruikshank, W. W., Foster, B., Prussin, C., Kirshenbaum, A. S., Davis, T. A., Kornfeld, H., Center, D. M., and Metcalfe, D. D. (1997) Human mast cells produce the CD4<sup>+</sup> T lymphocyte chemoattractant factor, IL-16. *J. Immunol.* **159**, 2904–2910
- Laberge, S., Cruikshank, W. W., Kornfeld, H., and Center, D. M. (1995) Histamine-induced secretion of lymphocyte chemoattractant factor from CD8<sup>+</sup> T cells is independent of transcription and translation: evidence for constitutive protein synthesis and storage. *J. Immunol.* **155**, 2902–2910
- Liu, Y., Cruikshank, W. W., O'Loughlin, T., O'Reilly, P., Center, D. M., and Kornfeld, H. (1999) Identification of a CD4 domain required for interleukin-16 binding and lymphocyte activation. *J. Biol. Chem.* **274**, 23387–23395
- Keane, J., Nicoll, J., Kim, S., Wu, D. M., Cruikshank, W. W., Brazer, W., Natke, B., Zhang, Y., Center, D. M., and Kornfeld, H. (1998) Conservation of structure and function between human and murine IL-16. *J. Immunol.* **160**, 5945–5954
- Richmond, J., Tuzova, M., Cruikshank, W., and Center, D. (2014) Regulation of cellular processes by interleukin-16 in homeostasis and cancer. *J. Cell. Physiol.* **229**, 139–147
- Wilson, K. C., Cruikshank, W. W., Center, D. M., and Zhang, Y. (2002) Prointerleukin-16 contains a functional CcN motif that regulates nuclear localization. *Biochemistry* **41**, 14306–14312
- Zhang, Y., Center, D. M., Wu, D. M., Cruikshank, W. W., Yuan, J., Andrews, D. W., and Kornfeld, H. (1998) Processing and activation of prointerleukin-16 by caspase-3. *J. Biol. Chem.* **273**, 1144–1149
- Cruikshank, W. W., Berman, J. S., Theodore, A. C., Bernardo, J., and Center, D. M. (1987) Lymphokine activation of T4<sup>+</sup> T lymphocytes and monocytes. *J. Immunol.* **138**, 3817–3823
- Center, D. M., Kornfeld, H., and Cruikshank, W. W. (1996) Interleukin 16 and its function as a CD4 ligand. *Immunol. Today* **17**, 476–481
- Little, F. F., and Cruikshank, W. W. (2004) Interleukin-16 and peptide derivatives as immunomodulatory therapy in allergic lung disease. *Expert Opin. Biol. Ther.* **4**, 837–846
- Lynch, E. A., Heijens, C. A., Horst, N. F., Center, D. M., and Cruikshank, W. W. (2003) Cutting edge: IL-16/CD4 preferentially induces Th1 cell migration: requirement of CCR5. *J. Immunol.* **171**, 4965–4968
- Glass, W. G., Sarisky, R. T., and Vecchio, A. M. (2006) Not-so-sweet sixteen: the role of IL-16 in infectious and immune-mediated inflammatory diseases. *J. Interferon Cytokine Res.* **26**, 511–520
- Bacon, K., Baggiolini, M., Broxmeyer, H., Horuk, R., Lindley, I., Mantovani, A., Maysushima, K., Murphy, P., Nomiyama, H., Oppenheim, J., et al. (2002) Chemokine/chemokine receptor nomenclature. *J. Interferon Cytokine Res.* **22**, 1067–1068
- Mühlhahn, P., Zweckstetter, M., Georgescu, J., Ciosto, C., Renner, C., Lanzendörfer, M., Lang, K., Ambrosius, D., Baier, M., Kurth, R., and Holak, T. A. (1998) Structure of interleukin 16 resembles a PDZ domain with an occluded peptide binding site. *Nat. Struct. Biol.* **5**, 682–686
- Harrison, S. C. (1996) Peptide-surface association: the case of PDZ and PTB domains. *Cell* **86**, 341–343
- Nicoll, J., Cruikshank, W. W., Brazer, W., Liu, Y., Center, D. M., and Kornfeld, H. (1999) Identification of domains in IL-16 critical for biological activity. *J. Immunol.* **163**, 1827–1832
- Santamaria, P. (2003) Cytokines and chemokines in autoimmune disease: an overview. *Adv. Exp. Med. Biol.* **520**, 1–7
- Conti, P., Kempuraj, D., Kandere, K., Di Gioacchino, M., Reale, M., Barbacane, R. C., Castellani, M. L., Mortari, U., Boucher, W., Letourneau, R., and Theoharides, T. C. (2002) Interleukin-16 network in inflammation and allergy. *Allergy Asthma Proc.* **23**, 103–108
- Stoitzner, P., Ratzinger, G., Koch, F., Janke, K., Schöller, T., Kaser, A., Tilg, H., Cruikshank, W. W., Fritsch, P., and Romani, N. (2001) Interleukin-16 supports the migration of Langerhans cells, partly in a CD4-independent way. *J. Invest. Dermatol.* **116**, 641–649
- Wang, S., Diao, H., Guan, Q., Cruikshank, W. W., Delovitch, T. L., Jevnikar, A. M., and Du, C. (2008) Decreased renal ischemia-reperfusion injury by IL-16 inactivation. *Kidney Int.* **73**, 318–326
- Spizizen, J. (1958) Transformation of biochemically deficient strains of *Bacillus subtilis* by deoxyribonucleate. *Proc. Natl. Acad. Sci. U.S.A.* **44**, 1072–1078
- Anagnostopoulos, C., and Spizizen, J. (1961) Requirements for transformation in *Bacillus subtilis*. *J. Bacteriol.* **81**, 741–746
- Hyberts, S. G., Milbradt, A. G., Wagner, A. B., Arthanari, H., and Wagner, G. (2012) Application of iterative soft thresholding for fast reconstruction of NMR data non-uniformly sampled with multidimensional Poisson Gap scheduling. *J. Biomol. NMR* **52**, 315–327
- Delaglio, F., Grzesiek, S., Vuister, G. W., Zhu, G., Pfeifer, J., and Bax, A. (1995) NMRPipe: a multidimensional spectral processing system based on UNIX pipes. *J. Biomol. NMR* **6**, 277–293
- Williamson, R. A., Carr, M. D., Frenkiel, T. A., Feeney, J., and Freedman, R. B. (1997) Mapping the binding site for matrix metalloproteinase on the N-terminal domain of the tissue inhibitor of metalloproteinases-2 by NMR chemical shift perturbation. *Biochemistry* **36**, 13882–13889
- Kabsch, W. (2010) Xds. *Acta Crystallogr. D Biol. Crystallogr.* **66**, 125–132
- Winn, M. D., Ballard, C. C., Cowtan, K. D., Dodson, E. J., Emsley, P., Evans, P. R., Keegan, R. M., Krissinel, E. B., Leslie, A. G., McCoy, A., McNicholas, S. J., Murshudov, G. N., Pannu, N. S., Potterton, E. A., Powell, H. R., et al. (2011) Overview of the CCP4 suite and current developments. *Acta Crystallogr. D Biol. Crystallogr.* **67**, 235–242
- Kantardjiev, K. A., and Rupp, B. (2003) Matthews coefficient probabilities: improved estimates for unit cell contents of proteins, DNA, and protein-nucleic acid complex crystals. *Protein Sci.* **12**, 1865–1871
- Schwede, T., Kopp, J., Guex, N., and Peitsch, M. C. (2003) SWISS-MODEL: an automated protein homology-modeling server. *Nucleic Acids Res.* **31**, 3381–3385
- Ma, J., Tang, W. K., Esser, L., Pastan, I., and Xia, D. (2012) Recognition of mesothelin by the therapeutic antibody MORAb-009: structural and mechanistic insights. *J. Biol. Chem.* **287**, 33123–33131
- Larsen, N. A., Zhou, B., Heine, A., Wirsching, P., Janda, K. D., and Wilson, I. A. (2001) Crystal structure of a cocaine-binding antibody. *J. Mol. Biol.* **311**, 9–15
- McCoy, A. J., Grosse-Kunstleve, R. W., Adams, P. D., Winn, M. D., Storoni, L. C., and Read, R. J. (2007) Phaser crystallographic software. *J. Appl. Crystallogr.* **40**, 658–674
- Emsley, P., and Cowtan, K. (2004) Coot: model-building tools for molecular graphics. *Acta Crystallogr. D Biol. Crystallogr.* **60**, 2126–2132
- Adams, P. D., Afonine, P. V., Bunkoczi, G., Chen, V. B., Davis, I. W., Echols, N., Headd, J. J., Hung, L. W., Kapral, G. J., Grosse-Kunstleve, R. W., McCoy, A. J., Moriarty, N. W., Oefner, R., Read, R. J., Richardson, D. C., et al. (2010) PHENIX: a comprehensive Python-based system for macromolecular structure solution. *Acta Crystallogr. D Biol. Crystallogr.* **66**, 213–221
- Murshudov, G. N., Vagin, A. A., and Dodson, E. J. (1997) Refinement of

## Structure of Interleukin-16 Bound to the 14.1 Antibody

- macromolecular structures by the maximum-likelihood method. *Acta Crystallogr. D Biol. Crystallogr.* **53**, 240–255
39. Addis, P. W., Hall, C. J., Bruton, S., Veverka, V., Wilkinson, I. C., Muskett, F. W., Renshaw, P. S., Prosser, C. E., Carrington, B., Lawson, A. W., Griffin, R., Taylor, R. J., Waters, L. C., Henry, A. J., and Carr, M. D. (2014) Conformational heterogeneity in antibody-protein antigen recognition: implications for high affinity protein complex formation. *J. Biol. Chem.* **289**, 7200–7210
  40. Lo Conte, L., Chothia, C., and Janin, J. (1999) The atomic structure of protein-protein recognition sites. *J. Mol. Biol.* **285**, 2177–2198
  41. Al-Lazikani, B., Lesk, A. M., and Chothia, C. (1997) Standard conformations for the canonical structures of immunoglobulins. *J. Mol. Biol.* **273**, 927–948
  42. Harris, B. Z., and Lim, W. A. (2001) Mechanism and role of PDZ domains in signaling complex assembly. *J. Cell Sci.* **114**, 3219–3231
  43. Ivanova, M. E., Fletcher, G. C., O'Reilly, N., Purkiss, A. G., Thompson, B. J., and McDonald, N. Q. (2015) Structures of the human Pals1 PDZ domain with and without ligand suggest gated access of Crb to the PDZ peptide-binding groove. *Acta Crystallogr. D Biol. Crystallogr.* **71**, 555–564
  44. Cruikshank, W. W., Center, D. M., Nisar, N., Wu, M., Natke, B., Theodore, A. C., and Kornfeld, H. (1994) Molecular and functional analysis of a lymphocyte chemoattractant factor: association of biologic function with CD4 expression. *Proc. Natl. Acad. Sci. U.S.A.* **91**, 5109–5113
  45. Lawson, A. D. (2012) Antibody-enabled small-molecule drug discovery. *Nat. Rev. Drug Discov.* **11**, 519–525
  46. Robert, X., and Gouet, P. (2014) Deciphering key features in protein structures with the new ENDscript server. *Nucleic Acids Res.* **42**, W320–W4

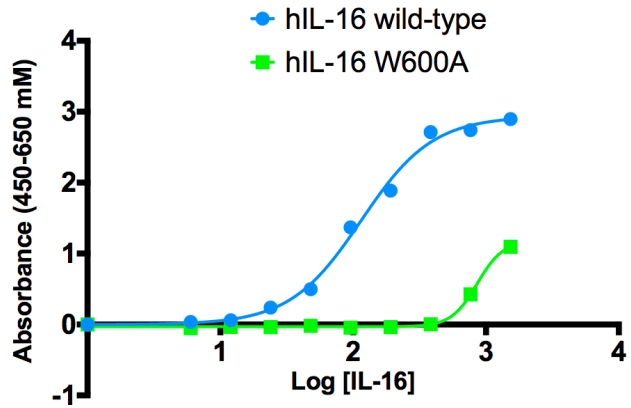
**SUPPLEMENTARY FIGURE 1. c14.1 antibody binding to plate-bound hIL-16 constructs using an ELISA-type binding assay.** Microtiter wells were coated with either hIL-16 (*closed blue circles*) or hIL-16 W600A (*closed green squares*) at various concentrations to determine their binding specificity for c14.1 antibody. The c14.1 antibody was detected using a secondary anti-Fc antibody conjugated to HRP (1:5000) and then developed. Data were analyzed by GraphPad Prism software. The ELISA binding study showed that mutating residue Trp600 to alanine in hIL-16 resulted in a ~10-fold increase in the EC<sub>50</sub> value from 115.1 nM to >858.7 nM, demonstrating the importance of Trp600 in the interaction interface.

**SUPPLEMENTARY FIGURE 2. Absence of a measurable direct interaction between hIL-16 and CD4 by NMR.** Shown are overlaid <sup>15</sup>N-<sup>1</sup>H HSQC spectra of <sup>15</sup>N-labelled hIL-16 both in the absence (blue) and presence (red) of recombinant unlabelled hCD4 domains D1-D4. The spectra overlay very closely, showing no discernable shifts in the spectra of <sup>15</sup>N-labelled hIL-16 in the presence of 5-molar excess of CD4, suggesting no interaction between hIL-16 and CD4.

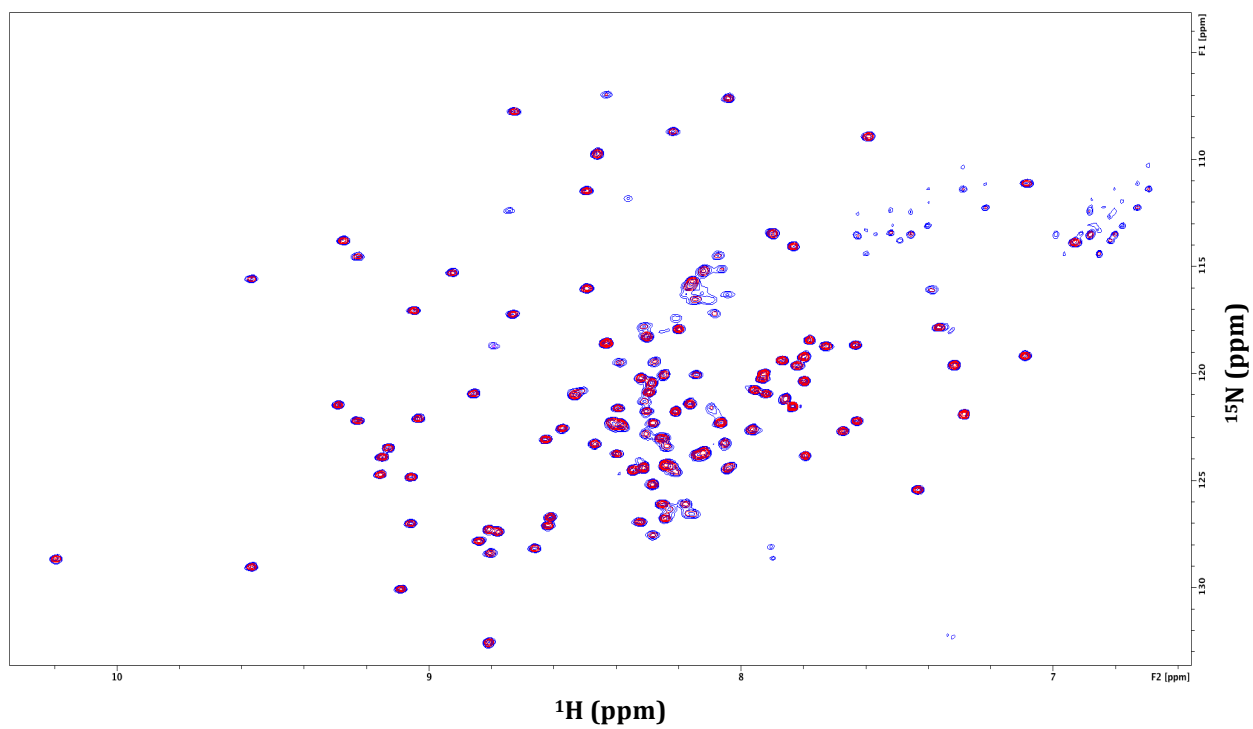
**SUPPLEMENTARY FIGURE 3. Lack of detectable binding of IL-16 to cell surface CD4.** (A) CD4 +ve Jurkat cells were stained with a dose response curve of Biotinylated IL-16 (33mg/mL, 3.3mg/mL, 300ng/mL, 33ng/mL, 3.3ng/mL) or Biotinylated OKT4 antibody, (500ng/mL) and subsequently detected with Streptavidin AlexaFluor 488. Red histograms OKT4 antibody staining, blue histograms biotinylated IL-16, green Streptavidin AlexaFluor 488 only. (B) Displacement of OKT4 from CD4+ve SupT1 cells. Red histograms OKT4 antibody staining, (500ng/mL), blue histograms hIL-16 dose response curve at 100mg/mL, 25mg/mL, 10mg/mL, 2.5mg/mL, 1mg/mL, green Streptavidin AlexaFluor 488 only. The FACS data indicate no direct binding of hIL-16 to CD4.

SUPPLEMENTARY FIGURE 1.

	hIL-16 wild-type	hIL-16 W600A
<b>Sigmoidal dose-response (variable slope)</b>		
<b>Best-fit values</b>		
<b>Bottom</b>	-0.001620	-0.03153
<b>Top</b>	2.937	1.181
<b>LogEC50</b>	2.061	2.934
<b>Hill Slope</b>	1.617	4.442
<b>EC50 (nM)</b>	115.1	858.7

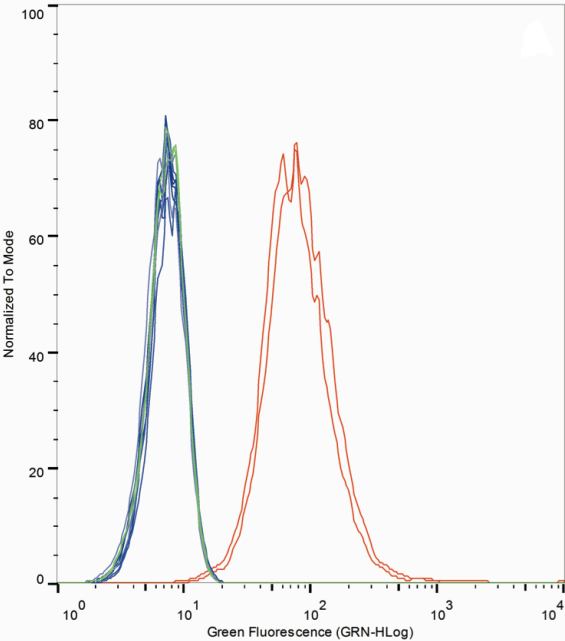


**SUPPLEMENTARY FIGURE 2.**

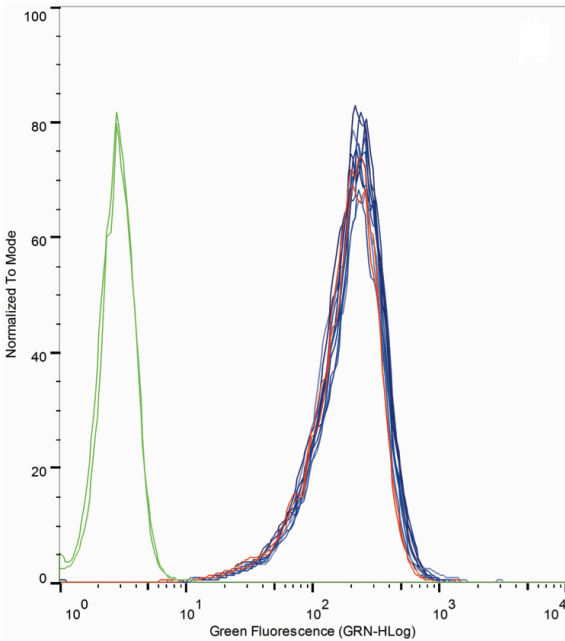


**SUPPLEMENTARY FIGURE 3.**

**A.**



**B.**



**Structure of a Potential Therapeutic Antibody Bound to Interleukin-16 (IL-16):  
MECHANISTIC INSIGHTS AND NEW THERAPEUTIC OPPORTUNITIES**  
Gareth Hall, Eilish Cullen, Kovilen Sawmynaden, Joanne Arnold, Simon Fox, Richard  
Cowan, Frederick W. Muskett, David Matthews, Andrew Merritt, Catherine  
Kettleborough, William Cruikshank, Debra Taylor, Richard Bayliss and Mark D. Carr

*J. Biol. Chem.* 2016, 291:16840-16848.

doi: 10.1074/jbc.M115.709303 originally published online May 26, 2016

---

Access the most updated version of this article at doi: [10.1074/jbc.M115.709303](https://doi.org/10.1074/jbc.M115.709303)

Alerts:

- [When this article is cited](#)
- [When a correction for this article is posted](#)

[Click here](#) to choose from all of JBC's e-mail alerts

Supplemental material:

<http://www.jbc.org/content/suppl/2016/06/14/M115.709303.DC1.html>

This article cites 46 references, 17 of which can be accessed free at  
<http://www.jbc.org/content/291/32/16840.full.html#ref-list-1>